RSC Advances

PAPER

View Article Online
View Journal | View Issue

Check for updates

Cite this: *RSC Adv.*, 2021, **11**, 31131

Synthesis of nano-zirconium-iron oxide supported by activated carbon composite for the removal of Sb(v) in aqueous solution†

Yanjun Liu, Lingda Meng, Kai Han and Shujuan Sun *

In this study, nano zirconium iron oxide based on activated carbon (ZIC) was successfully prepared by using the coprecipitation method. Compared with unmodified activated carbon, ZIC increases the number of active sites by adding metal oxides and hydroxyl groups and greatly improves the adsorption capacity of Sb(v). The synthesized nanocomposites were characterized and analysed by XRD, SEM, FT-IR, VSM and other techniques. The results showed that the zirconium iron oxide particles were successfully loaded and uniformly distributed on the surface of the activated carbon, and the agglomeration phenomenon was reduced. The saturation magnetization of ZIC was 1.89 emu g^{-1}, which easily achieved solid–liquid separation under the action of an external magnetic field. In batch experiments, when the initial concentration was 1 mg L^{-1}, the dosage of ZIC was 600 mg L^{-1}, the pH value was 5.0, the contact time was 180 min, and the removal rate of Sb(v) reached 97.82%. The maximum adsorption capacity of ZIC for Sb(v) was 11.80 mg g^{-1}. Under the interference of various inorganic ions and dissolved organics, the excellent adsorption capacity was still due to ZIC. The adsorption form was multimolecular-layer adsorption, the adsorption process was an endothermic reaction, and chemical adsorption was dominant as the adsorption mechanism. ZIC has good removal efficiency and is reusable, which indicates that ZIC has prospects for practical wastewater treatment.

Received 13th August 2021
Accepted 9th September 2021

DOI: 10.1039/d1ra06117h

rsc.li/rsc-advances

Open Access Article. Published on 20 September 2021. Downloaded on 2/13/2026 11:42:16 PM.
This article is licensed under a Creative Commons Attribution-NonCommercial 3.0 Unported Licence.

1. Introduction

As the world's largest antimony reserve and production country, China accounts for approximately 71 percent of the world's total production. Due to the influence of human activities and the widespread use of antimony compounds, antimony pollution has become a typical environmental pollution problem in China.[1] Antimony (Sb) is a metalloid that ubiquitously exists in the environment at trace levels, and its compounds have potential toxicity and carcinogenicity. Sb is also listed as a priority pollutant by the United States Environmental Protection Agency (USEPA). Direct or indirect contact with antimony-contaminated water can lead to antimony poisoning, causing serious harm to environmental organisms and human health.[2,3] Sb(III) and Sb(v) usually exist in natural water environments. In most oxidized waters, antimony mainly exists in the anionic form of $Sb(OH)_6^-$, and its risk is much higher than that of other forms. Therefore, it is urgently needed to develop advanced Sb(v)-removal technology in water environments.

The adsorption method is considered to be a simple, economical and environmentally friendly, antimony-removal technology. The type and performance of the adsorbents directly affect the adsorption efficiency. As a traditional material for adsorbing environmental contaminants, activated carbon has attracted much attention for its advantages, such as widespread sources, low price, large specific surface area, and abundant functional groups on the surface.[4] Long *et al.*[5] summarized recent research progress on antimony removal and concluded that modified activated carbon has a better adsorption effect than pure activated carbon. Adsorption performance could be improved through metal-based materials or other improvements. Bessaies *et al.*[6] used modified carbon-based materials to effectively remove antimony in aqueous solutions, with an adsorption capacity of 77.72 mg g^{-1}. Deng *et al.*[7] prepared amino-functional, activated carbon that can simultaneously adsorb Cr(vi) and Sb(v) in aqueous solution. In addition, it has a strong anti-interference ability against coexisting inorganic ions and humus.

In addition to carbon-based materials, some metal oxides are widely used to repair heavy metal pollution due to their advantages of simple preparation, low cost, nontoxicity, harmlessness and high environmental friendliness.[8] At present, magnetic nanoiron-based oxides have been successfully developed as new adsorbents. Compared with traditional adsorbents, they have the advantages of low diffusion resistance, a large specific surface, high adsorption efficiency, rapid separation and recycling. They overcome the difficulty of traditional

College of Resources and Environment, Shandong Agricultural University, Taian, Shandong, 271018, China. E-mail: sunsjnk@sdau.edu.cn; Tel: +86-138-54867706

† Electronic supplementary information (ESI) available. See DOI: 10.1039/d1ra06117h

© 2021 The Author(s). Published by the Royal Society of Chemistry

Open Access Article. Published on 20 September 2021. Downloaded on 2/13/2026 11:42:16 PM.
This article is licensed under a Creative Commons Attribution-NonCommercial 3.0 Unported Licence.

adsorbent recovery and they reduce the risk of secondary pollution to the environment. Qi *et al.*[9] synthesized Ce(III)-doped magnetic iron-oxide ions, which can effectively remove antimony from aqueous solution and can quickly perform solid–liquid separation. In addition, zirconia is considered to be one of the most promising adsorbents for antimony removal in water environments due to its excellent chemical stability, nontoxicity and insolubility in water environments. Li *et al.*[10] used the coprecipitation method to synthesize Fe–Zr binary oxide as an Sb(v) adsorbent, and its adsorption capacity was better than that of iron oxide and zirconium oxide. Compared with single metal oxides, binary oxides often exhibit better adsorption performance in adsorbing Sb(v).

Therefore, this work mainly studies the preparation and characterization of nano-zirconium iron oxide based on activated carbon (ZIC), as well as the removal effect and adsorption mechanism of Sb(v) in water. The main contents include (1) determination of preparation conditions: exploring the optimal proportion of zirconium-iron content in the process of preparing ZIC composites; (2) material characterization: using FT-IR, SEM and XRD characterization methods to characterize and analyse ZIC and studying its composition, morphology, and loading mode; and (3) batch experiment: studying the adsorption performance of ZIC on Sb(v) in aqueous solution, analysing the influence of single factors, such as pH value, initial concentration of Sb(v), adsorbent dosage, experimental temperature and time, on the adsorption effect, and discussing the adsorption mechanism and regeneration capacity.

2. Materials and methods

2.1 Materials

All chemicals were of AR or higher grade. Potassium pyroantimonate ($KSb(OH)_6$), zirconium oxychloride ($ZrOCl_2 \cdot 8H_2O$) and humic acid (HA) were purchased from the Shanghai Macklin Biochemical Co., Ltd. Commercial activated carbon was purchased from Tianjin Kaitong Chemical Reagent Co., Ltd. Other chemicals were purchased from the China National Medicines Corporation, Ltd. Stock solutions (1000 mg L^{-1}) of Sb(v) were prepared by dissolving $KSb(OH)_6$ in deionized water (DI). Other Sb(v) solutions were obtained by diluting the 1000 mg L^{-1} Sb(v) stock solution with deionized water.

2.2 Preparation and optimization of adsorbents

Activated carbon pretreatment. A certain amount of activated carbon was sieved through a 60-mesh sieve to screen out activated carbon with a particle size greater than 0.25 mm. The activated carbon was washed with 1 M hydrochloric acid solution for 2 h to remove ash. After pickling, the activated carbon was repeatedly washed with deionized water until it was neutral. Washing the material ensures that there is no hydrochloric acid residue. The washed material was dried at 105 °C to a constant weight, and the obtained activated carbon was reserved.

Adsorbent preparation method and optimization of preparation conditions. Two grams of activated carbon was added to 300 mL of deionized water and anhydrous ethanol mixed solution at a volume ratio of 1 : 1, and ultrasonic treatment was performed for 1 hour to uniformly disperse the activated carbon to form a suspension. Then, 0.056 g $FeSO_4 \cdot 7H_2O$, 0.040 g $FeCl_3$, and 0.096 g $ZrOCl_2 \cdot 8H_2O$ (zirconium-iron molar ratio 1 : 1) were added to the reaction system. Under nitrogen protection, an appropriate amount of 5 M NaOH solution was added dropwise to the reaction system, and the pH value was adjusted to 10.0. After ultrasound for 1 h, it was transferred to a polytetrafluoroethylene lining and then loaded into a high-temperature reactor. It was put into a vacuum-drying oven and reacted at 180 °C for 9 h. After the reactor was naturally cooled, the product was separated from the reaction liquid by a magnet, and the material was repeatedly washed with deionized water to neutrality. The material was placed in a vacuum-drying oven at 90 °C to be dried to a constant weight, sealed and dried for later use, thus obtaining a ZIC composite material. The composite material with a molar ratio of zirconium to iron of 1 : 3 and 1 : 5 were prepared by the same steps.

2.3 Characterization

In this experiment, an inductively coupled plasma spectrometer (Thermo Scientific ICAP 7000) was used to measure the concentration of antimony in the solution at 206.83 nm. An automatic specific surface area and porosity analyser (Micromeritics ASAP 2020 HD88; Quantachrome Autosorb-iQ) was used, the adsorbate was N_2, the adsorption temperature was 200 °C, and the degassing treatment was heated for 4 hours to obtain the N_2 adsorption isotherm of the sample. The Brunauer–Emmett–Teller (BET) method was used to calculate the specific surface area based on the adsorption isotherm. The pore size and pore volume were obtained by using the Barrett–Joyner–Halenda (BJH) model. A scanning electron microscope (Zeiss Sigma 300) was used to observe the surface morphology of the sample. An X-ray diffractometer (Bruker D8 Advance) was used to analyse the structure of the samples, and the scanning speed was 5° min^{-1}. The surface functional groups of the adsorbents were determined by FTIR spectroscopy (Thermo Scientific Nicolet 10). A vibrating sample magnetometer (Lake-Shore7404) was used to measure the magnetic properties of the sample under the condition that the sample was vibrated perpendicular to the uniform magnetization field at room temperature, and the magnetic field was within ±3 T.

2.4 Batch experiments

Utilizing batch adsorption experiments, the removal rate of Sb(v) was used as an indicator to determine the best ratio of zirconium to iron in the ZIC. We further explored the effect of adsorbent dosage, pH value, adsorption kinetics, adsorption isotherm, adsorption thermodynamics, coexisting ions (Cl^-, SO_4^{2-}, and PO_4^{3-}), and dissolved organic matter (HA) on Sb(v) adsorption. Finally, adsorption and desorption experiments were carried out to study the reusability and regeneration potential of the adsorbent. All the experiments were carried out in triplicate, and average values are used in this paper. The experimental steps are recorded in Text S1.†

© 2021 The Author(s). Published by the Royal Society of Chemistry

Open Access Article. Published on 20 September 2021. Downloaded on 2/13/2026 11:42:16 PM.
This article is licensed under a Creative Commons Attribution-NonCommercial 3.0 Unported Licence.

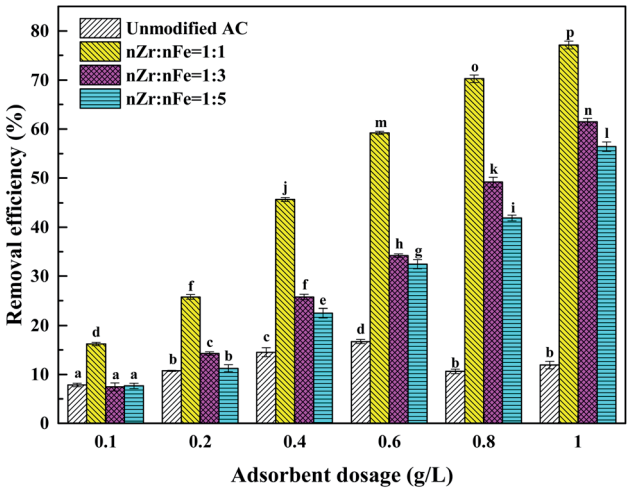

Fig. 1 The influence of different load conditions on the removal of Sb(v) (initial concentration, 1 mg L^{-1}; pH value, 7.0; temperature, 298 K; contact time, 180 min; and rpm, 160). Note: different lowercase letters indicate significant differences among treatments at p <0.05, the same as below.

3. Results and discussion

3.1 The influence of iron-zirconium molar ratio on adsorption

Under the conditions of an initial Sb(v) concentration of 1 mg L^{-1}, a temperature of 298 K and a pH value of 7, the effects of different loading conditions on the removal of Sb(v) were studied. The experimental results are shown in Fig. 1 and Table S1.†

According to the data, the removal rate of Sb(v) by unmodified activated carbon was 11.91%. The unmodified activated carbon has a poor adsorption effect on Sb(v), which may be caused by its high ash content and small pore capacity.[11] In view of the fact that the surface functional groups of unmodified activated carbon cannot produce a good adsorption effect on Sb(v), this proves the necessity of modifying activated carbon in the experiment. Due to the addition of metal oxides and hydroxyl groups on the surface of the material and the increase in active sites, the adsorption capacity of ZIC to Sb(v) is greatly improved compared with unmodified activated carbon.[12] When the molar ratios of iron to zirconium ions in the ZIC were 1 : 1, 1 : 3 and 1 : 5, the removal rates of Sb(v) were 77.11%, 61.49% and 56.4%, respectively. The surface of zirconia has a special pore structure, which is favourable to the diffusion of Sb(v) in the pores. Due to the unique affinity between zirconium and antimony,[13] the adsorption effect is better when the zirconium content is high. In summary, modified activated carbon with a molar ratio of zirconium to iron ions of 1 : 1 will be selected for a series of characterization and adsorption tests.

3.2 Adsorbent characterization

The N_2 adsorption–desorption curve and the pore size distribution curve of ZIC are shown in Fig. S1 and S2.† According to the IUPAC classification, N_2 adsorption–desorption curves belong to type IV and type H3 hysteresis loops, indicating the presence of mesopores in the sample.[14] Since the adsorption capacity of the H3-type hysteresis ring is not limited when the relative pressure is high, the void structure of ZIC is mainly the holes produced by the aggregation of particles. The ZIC prepared in this experiment has a pore diameter in the range of 3.053–70.155 nm, an average pore diameter of 3.848 nm, a porosity of 0.036 $cm^3\ g^{-1}$, a BET method specific surface area of 23.989 $m^2\ g^{-1}$, a Langmuir method specific surface area of 19.409 $m^2\ g^{-1}$, and a specific surface area higher than that of unmodified AC.[15] Therefore, ZIC has a larger specific surface area, more hollow structure and smaller nanoscale size than AC, which are conducive to its adsorption of Sb(v) in water.

Scanning electron micrographs of unmodified activated carbon and ZIC are shown in Fig. 2. The unmodified activated carbon has a smooth surface, numerous pores, and an irregular porous structure. Compared with the unmodified activated carbon, the ZIC composite material is composed of block activated carbon and spherical particles. The nanoparticles are distributed along the pores of activated carbon, wherein clusters with sizes of 62–109 nm consisting of smaller sized (43–51 nm) Fe–Zr nanoparticles are observed. When the nanoparticles are closely attached to the activated carbon, the surface of the adsorbent is rougher. This shows that the nanoparticles are successfully loaded on the surface of the activated carbon and distributed evenly, which reduces the reunion phenomenon.[12]

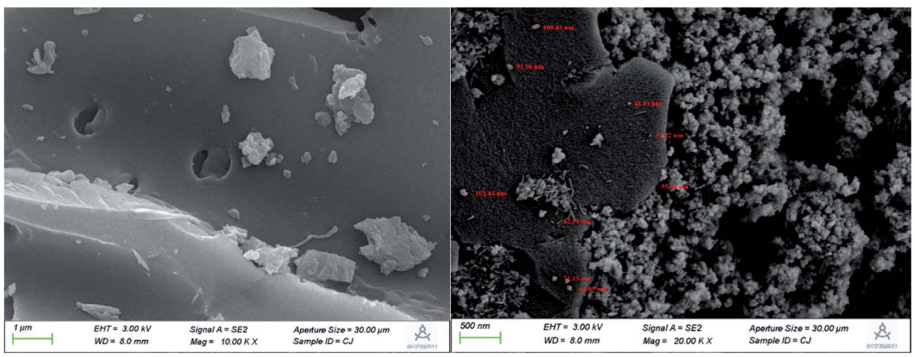

Fig. 2 SEM patterns of unmodified AC (left) and ZIC (right).

Open Access Article. Published on 20 September 2021. Downloaded on 2/13/2026 11:42:16 PM.
This article is licensed under a Creative Commons Attribution-NonCommercial 3.0 Unported Licence.

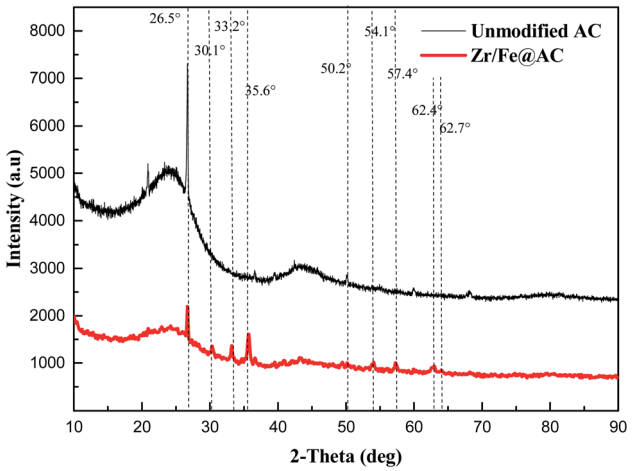

Fig. 3 XRD patterns of unmodified AC and ZIC.

Moreover, some particles enter the pores of activated carbon, which has stronger adhesion and does not easily fall off, which makes the ZIC nanocomposite material stable.

The XRD spectra of unmodified activated carbon and ZIC are shown in Fig. 3. The unmodified activated carbon can be observed to show the diffraction peak of carbon when 2θ is 26.5°, and then there is no obvious diffraction peak of 2θ in the range of 30.0–90.0°, indicating that the unmodified activated carbon is composed of crystalline carbon structure and amorphous carbon structure.[16] The carbon diffraction peak of ZIC at a 2θ of 26.5° is smaller, which makes the carbon structure change from crystalline to amorphous. It may be that the original crystal structure of activated carbon is destroyed by the loading of zirconium iron binary oxide, or the necessary conditions for the formation of activated carbon crystal are destroyed.[12] Since the amorphous sample has larger pores, smaller structure and more adsorption sites, the pollutant ions in the solution can diffuse to the surface of the composite material and the voids more quickly, thereby contributing to the adsorption of antimony ions.[16,17] By comparing and analysing with the JCPDS card, it can be seen that the characteristic peaks of γ-Fe_2O_3 and Fe_3O_4 are displayed at a 2θ of 35.6°, 54.1°, 57.4° and 62.9°,[18] and ZrO_2 at a 2θ of 30.1°, 33.2° and 50.2°.[19] This indicates that the main components of the adsorption material are activated carbon, magnetite, maghemite and zirconium dioxide.[20]

The magnetic strength of ZIC can be explored through VSM, and the magnetic characteristics of the adsorbent can be analysed. The results are shown in Fig. S3.† In the range of magnetic field strength ±3 T, the magnetic surface becomes more obvious as the magnetic field strength increases. When the material reaches magnetic saturation, the parameter curve is close to parallel to the *x*-axis. The saturation magnetization of ZIC is 1.89 emu g^{-1}, the magnetism exhibits superparamagnetic behaviour, and there is no remanence or coercivity.[13] It can still be quickly separated from the environment in an externally enhanced magnetic environment.

3.3 Adsorption performance

3.3.1 Effect of adsorbent dosage on adsorption. The adsorbent dosage is one of the important factors that affect the adsorption effect. The removal rate and adsorption capacity of the target pollutant Sb(v) will show regular changes with the dosage of ZIC. The results are shown in Fig. S4.† As the dose of ZIC increased from 100 mg L^{-1} to 600 mg L^{-1}, the removal rate of Sb(v) increased from 44.44% to 94.47%, and the adsorption capacity decreased from 4.44 mg g^{-1} to 1.58 mg g^{-1}. The dosage continued to increase to 2000 mg L^{-1}, and the adsorption capacity showed a steady decline. The final removal rate of Sb(v) was 99.81%, and the adsorption capacity was 0.4991 mg g^{-1}. The reason for this may be that the increase in dosage increases the total surface area of the adsorbent, and the adsorbent surface provides more active sites.[21] A large number of active sites promote the adsorption process so that the removal rate is stably improved. As the overall adsorption capacity of the adsorbent increases, the total surface area also increases, and its growth rate is far less than the latter, which weakens the adsorption capacity per unit area of the material, resulting in the adsorption capacity gradually decreasing. In summary, to ensure adsorption efficiency and economic benefits, the optimal dosage of adsorbents in the adsorption experiment was 600 mg L^{-1}, and the removal rate was 94.47%.

3.3.2 Effect of pH valve on adsorption. The pH value of the solution will directly affect the morphology of the adsorbate and the surface charge of the adsorbent, which in turn affects the overall adsorption performance of the adsorbent for Sb(v).

Fig. 4 shows that the removal rate of Sb(v) by ZIC decreases with increasing solution pH. When the pH value of the solution was 4–5, the adsorption capacity of ZIC was higher, and the removal rate ranged from 97.35 to 97.82%. In the wide pH range (4.0–10.0), the adsorption capacity decreased with increasing pH value. When the pH value was 10, the removal rate was 44.13%. Under acidic conditions, the removal rate of Sb(v) by ZIC was stable.[22] With the increase in the pH value of the solution, the removal rate of Sb(v) decreased gradually. When

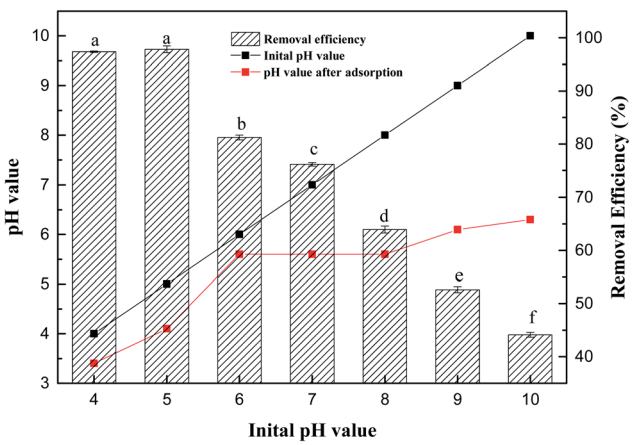

Fig. 4 The effect of different solution pH value on the adsorption of Sb(v) (initial concentration, 1 mg L^{-1}; absorbent dosage, 600 mg L^{-1}; temperature, 298 K; contact time, 180 min; and rpm, 160).

© 2021 The Author(s). Published by the Royal Society of Chemistry

Open Access Article. Published on 20 September 2021. Downloaded on 2/13/2026 11:42:16 PM.
This article is licensed under a Creative Commons Attribution-NonCommercial 3.0 Unported Licence.

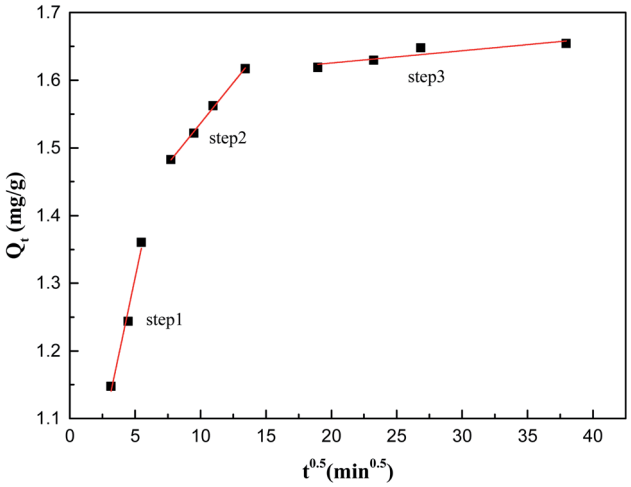

Fig. 5 The intraparticle diffusion model for Sb(v) removal on ZIC.

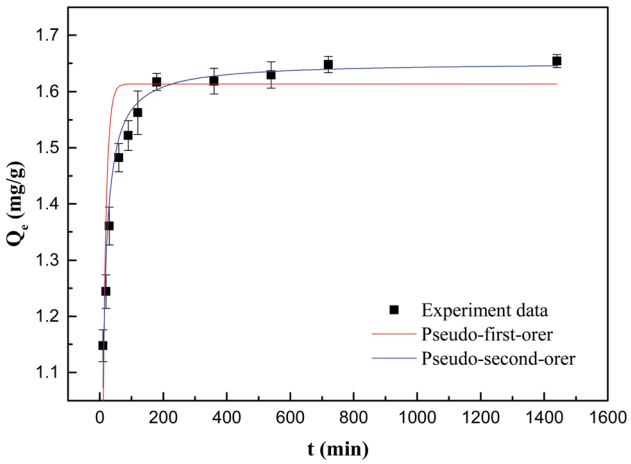

Fig. 6 The adsorption kinetic curve for Sb(v) removal on ZIC.

the pH value of the solution was 4–5, the adsorption capacity of ZIC was higher, and the removal rate was between 97.35 and 97.82%. Subsequently, the adsorption capacity decreased as the pH value increased. When the pH value was 10, the removal rate was 44.13%. It can be concluded that the best results can be obtained in an environment with a pH value of 5. In addition, according to the pH change of the solution before and after the experiment, it can be inferred that the surface charge of ZIC was positive, and pH_{zpc} <5.6.[23] When the pH value was ≤5.6, the positively charged ZIC surface had a strong attraction to the negatively charged adsorbate; when the pH value was >5.6, the surface charge of the ZIC became negatively charged, and electrostatic repulsion started to inhibit the adsorption process.[24] Considering that ZIC can still maintain a certain adsorption capacity in high pH solutions, it can be speculated that electrostatic interactions are an important factor of adsorption, but they are not the only mechanism.[25]

3.3.3 Adsorption kinetics. The effect of different contact times on adsorption is shown in Fig. S5.† As the contact time between ZIC and Sb(v) increased, the adsorption reaction gradually approached adsorption equilibrium. The adsorption process can be generally divided into two parts:[14] the first part is the rapid adsorption process. When the reaction time was 180 min, the adsorption process was close to adsorption saturation, and the removal rate of Sb(v) was 97.30%. The strong electrostatic interaction between the basic groups on the surface of ZIC and Sb(v) in the solution was the reason for the high initial adsorption rate in the adsorption process. The adsorption process involved mainly electrostatic interactions. The second part is the slow adsorption process. Within the range of 180–1440 min, the removal rate of Sb(v) did not change significantly, and the removal rate was 97.30–99.24%. As the reaction time increased, the active sites on the surface of the adsorbent became saturated, the Sb(v) ionic strength decreased, and the adsorption rate continued to decrease until adsorption equilibrium.[26] The adsorption process was mainly in the form of intraparticle diffusion.[27]

To further explore the adsorption reaction mechanism, the experimental data were fitted with the intraparticle diffusion model, the pseudo-first-order kinetic model and the pseudo-second-order kinetic model. The adsorption of Sb(v) on ZIC can be determined in three steps, and the surface adsorption is controlled by intraparticle diffusion.[28] The intraparticle diffusion model determines whether intraparticle diffusion is the only rate-limiting step in the adsorption process by observing the linear relationship between Q_t and $t^{0.5}$.

From Fig. 5 and Table S2,† it can be observed that the adsorption of Sb(v) on ZIC can be determined in three stages: (1) surface diffusion stage; (2) intraparticle diffusion stage; and (3) adsorption saturation stage. Since Q_t and $t^{0.5}$ are not linear through the origin, combined with the analysis of the pseudo-second-order kinetic model, it can be understood that the adsorption rate of Sb(v) on ZIC is not only based on intraparticle diffusion but also depends on other chemical adsorption processes.

The kinetic model and parameters of Sb(v) adsorption by ZIC are described, as shown in Fig. 6 and Table 1. The correlation coefficient of the model indicates that the pseudo-second-order kinetic model is very suitable for simulating the adsorption of Sb(v) with contact time. This means that according to previous research, adsorption may not only be limited to electrostatic

Table 1 Pseudo-first-order and pseudo-second-order kinetic model parameters

	Pseudo-first-order kinetic			Pseudo-second-order kinetic		
$Q_{e(exp.)}$ (mg g^{-1})	k_1 (min^{-1})	$Q_{e(cal.)}$ (mg g^{-1})	R^2	k_2 (mg^{-1} min^{-1})	$Q_{e(cal.)}$ (mg g^{-1})	R^2
1.6540	0.0958	1.6138	0.7113	5.3840	1.6510	0.9600

Open Access Article. Published on 20 September 2021. Downloaded on 2/13/2026 11:42:16 PM.
This article is licensed under a Creative Commons Attribution-NonCommercial 3.0 Unported Licence.

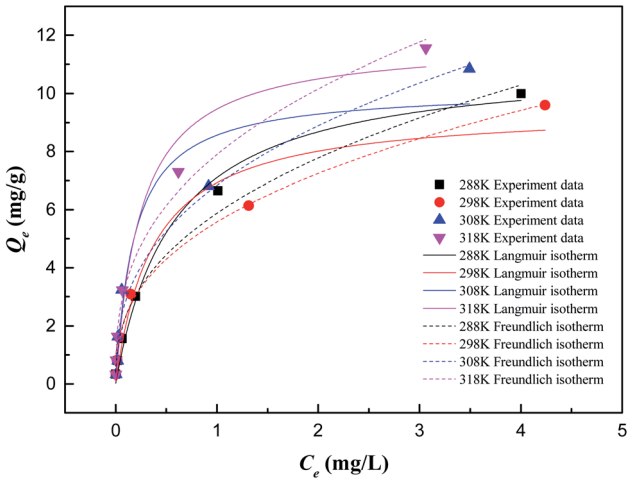

Fig. 7 The adsorption isotherm for Sb(v) removal on ZIC.

adsorption, but may also involve chemical adsorption between adsorbents and pollutants.[29,30]

3.3.4 Adsorption isotherm. During the adsorption process of ZIC composite material to Sb(v), the removal rate and adsorption capacity of Sb(v) will change with the change of the initial Sb(v) concentration. The effect of different initial Sb(v) concentrations on the adsorption is shown in Fig. S6.† With the continuous increase in the initial Sb(v) concentration, the removal rate continuously decreased. When the initial Sb(v) concentration was in the range of 0.2–2 mg L^{-1}, the removal rate of Sb(v) by ZIC was above 90%; when the initial concentration increased to the maximum test range of 10 mg L^{-1}, the removal rate was 57.62–69.36%. When the concentration of Sb(v) in the solution was low, the adsorption capacity of the material was also low, often not more than 1 mg g^{-1}. With increasing Sb(v) concentration, the adsorption capacity of the adsorbent also increased. The final adsorption capacity ranged from 9.60 to 11.56 mg g^{-1}. These results indicate that as the concentration of Sb(v) increases, the driving force of Sb(v) increases. Thus, the resistance of Sb(v) ions from the solution to the surface of the adsorbent is overcome, resulting in an increase in the adsorption capacity of ZIC. To further understand the interaction between Sb(v) and ZIC, Langmuir and Freundlich isotherm models were used to analyse the data (Fig. 7).

According to the fitting parameters in Table 2, both the Langmuir and Freundlich isotherm models can describe the adsorption process well. The Langmuir adsorption isotherm model assumes that the adsorption process takes place on a homogeneous surface. All active sites on the ZIC surface have the same adsorption capacity on Sb(v), and the removal rate will not change due to changes in the concentration of Sb(v) in the solution.[31] The adsorption process is single-layer adsorption. The Freundlich adsorption isotherm model assumes that the adsorption process occurs on a nonhomogeneous surface, the removal rate will increase with increasing Sb(v) concentration, and the adsorption process is multilayer adsorption.[32] In the Langmuir model, the theoretical maximum adsorption capacity of ZIC can be obtained as 11.80 mg g^{-1}, and the obtained K_L value indicates that there is a good interaction between Sb(v) and ZIC in the temperature range of 288–318 K. The R_L value is close to zero, indicating that the adsorption process easily proceeds within the experimental temperature range. In the Freundlich model, it can be seen from K_F that the adsorption capacity increases with increasing temperature. The value of $1/n$ is in the range of 0 to 1, which also indicates that the adsorption process easily proceeds.[5] This result might indicate that the heterogeneous surface energies by a multilayer adsorption could be used to describe adsorption behavior of Sb(v) on ZIC, and similar fitting results have been observed before.[33–35] Compared with other adsorbents, ZIC has a higher adsorption capacity. For example, the adsorption capacity of ZIC is 11.80 mg g^{-1} (the initial concentration of Sb(v) is 1 mg L^{-1}) is better than kaolinite (Q_m = 0.13 mg g^{-1}),[36] bentonite (Q_m = 0.50 mg g^{-1}),[37] ferrosoferric oxide (Q_m = 7.06 mg g^{-1})[38] and polyvinyl alcohol-stabilized granular adsorbent containing nanoscale zero-valent iron (Q_m = 1.65 mg g^{-1}).[34] This adsorption capacity is still lower than zirconium oxide -carbon nanofibers (Q_m = 51.17 mg g^{-1}),[35] reduced graphene oxide coupled with Mn_3O_4(Q_m = 105.50 mg g^{-1})[39] and α-MnO_2 Nanofibers (Q_m = 89.99 mg g^{-1}),[40] but the cost of ZIC is lower than these materials and has the advantage of magnetic separation.

3.3.5 Adsorption thermodynamics. Temperature is one of the important factors affecting the adsorption process. The influence of different ambient temperatures on the adsorption is shown in Fig. S7.† In this experiment, the adsorption process was promoted with increasing temperature, which may have been due to a decrease in the viscosity of the aqueous medium, which resulted in increased ionic diffusion.[41] Within the experimental temperature range, the removal rate of Sb(v) by ZIC increased from 93.65% to 98.23%. The adsorption reaction can be judged to have been an endothermic process.

Table 2 The adsorption isotherm parameters

Temperature (K)	Langmuir isotherm				Freundlich isotherm		
	Q_m (mg g^{-1})	K_L (L mg^{-1})	R_L	R^2	K_F (mg g^{-1})	$1/n$	R^2
288	11.1540	1.7530	0.1113	0.9868	5.8777	0.4043	0.9835
298	9.5004	2.6896	0.0866	0.9335	5.5758	0.3784	0.9930
308	10.1574	5.3690	0.1144	0.9230	6.8372	0.3789	0.9716
318	11.8035	4.0467	0.0716	0.9585	7.8974	0.3632	0.9829

© 2021 The Author(s). Published by the Royal Society of Chemistry

Open Access Article. Published on 20 September 2021. Downloaded on 2/13/2026 11:42:16 PM.
This article is licensed under a Creative Commons Attribution-NonCommercial 3.0 Unported Licence.

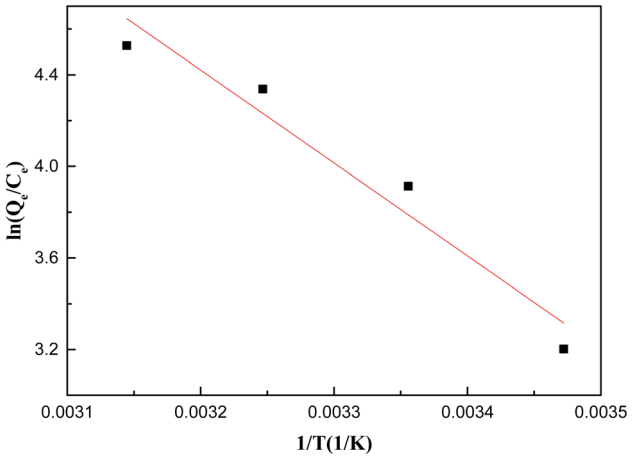

Fig. 8 The adsorption thermodynamic curve for Sb(v) removal on ZIC.

Fig. 8 and Table S3† provide thermodynamic information to evaluate thermodynamic feasibility and properties in the adsorption process. According to the correlation coefficient R^2 = 0.9217, the thermodynamic parameters conform to the thermodynamic equation. ΔH was a positive value, indicating the endothermic reaction of the adsorption process, and the conclusion is consistent with the adsorption isotherm data. Soluble Sb(v) needs to be dehydrated to specifically bind to ZIC. When the energy required for the dehydration process exceeds the exothermicity of the ions attached to the surface, the high temperature provides more energy for the dehydration of Sb(v) and provides more activation energy for single-layer chemical adsorption.[42] ΔG was a negative value, indicating that the adsorption process can proceed spontaneously within the test range, and higher temperatures can promote adsorption. ΔS was a positive value, indicating that the solid–liquid reaction surface in the reaction system has a high degree of freedom, which is advantageous and tends to spontaneously react. The adsorption of Sb(v) on the solid–liquid interface of ZIC is positive, which reflects the affinity of the adsorbent to Sb(v). There are some structural changes in the Sb substance and adsorbent. The adsorbent functional groups (hydroxyl and carboxy) and the M-O on the surface are protonated, which causes the adsorbent to generate a positive surface charge at acidic pH and promote Sb(v) adsorption. The results show that the Sb(v)–ZIC interaction is feasible at higher temperatures, which indicates that high temperatures are more beneficial to the adsorption process.[23]

3.3.6 Effect of co-existing anions on adsorption. There are many kinds of anions in natural water environments,[43] such as chloride, sulfate and phosphate. These anions may compete with Sb(v) for adsorption during practical applications. Therefore, experiments on the effect of coexisting anions on the adsorption effect were carried out to analyse the effect of chloride, sulfate and phosphate on the adsorption effect of Sb(v) under the same concentration conditions.

As shown in Fig. 9, chloride and sulfate had no significant effect on the removal process of Sb(v). Although their initial concentration (10 mg L^{-1}) was much higher than the concentration of Sb(v), no obvious negative effects of chloride and sulfate on adsorption were observed. The removal rates of Sb(v) by ZIC were 93.4% and 87.4%, respectively, which indicated that their competition for active sites on ZIC was weak.[44] In addition, phosphate had a greater impact on the removal process. When the initial concentrations of phosphate and Sb(v) were equal (1 mg L^{-1}), the removal rate of Sb(v) by ZIC was 73.95%; when the concentration of phosphate was increased to 10 mg L^{-1}, the removal rate was 42.47%. This may have been due to the competitive adsorption between phosphorus ions and antimony ions. In the periodic table, phosphorus and antimony are elements in the same main group, and phosphate and antimonate have similar molecular structures.[45] Phosphate and antimonate compete for adsorption at limited active sites, resulting in a significant decrease in the removal rate of Sb(v). In

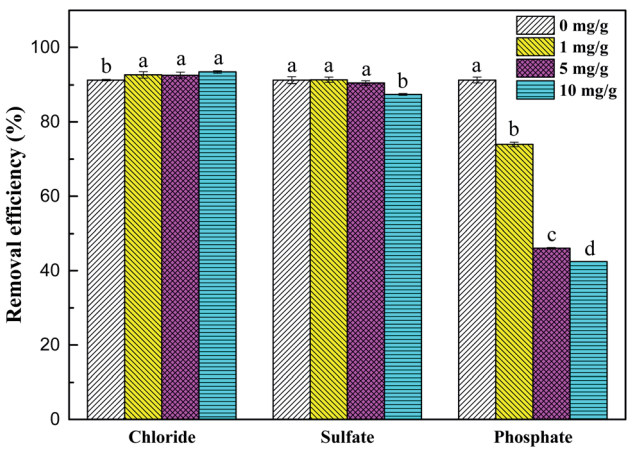

Fig. 9 The effect of co-existing ions on the adsorption of Sb(v) (initial concentration, 1 mg L^{-1}; pH value, 5.0; absorbent dosage, 600 mg L^{-1}; temperature, 298 K; contact time, 180 min; and rpm, 160).

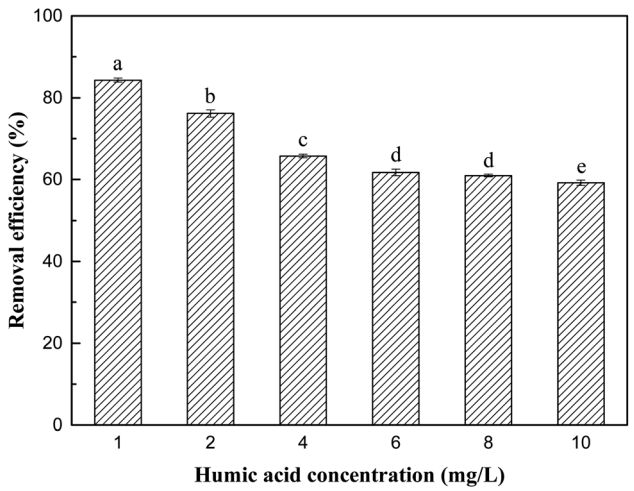

Fig. 10 Effect of humic acid on the adsorption of Sb(v) (initial concentration, 1 mg L^{-1}; pH value, 5.0; absorbent dosage, 600 mg L^{-1}; temperature, 298 K; contact time, 180 min; and rpm, 160).

© 2021 The Author(s). Published by the Royal Society of Chemistry

Open Access Article. Published on 20 September 2021. Downloaded on 2/13/2026 11:42:16 PM.
This article is licensed under a Creative Commons Attribution-NonCommercial 3.0 Unported Licence.

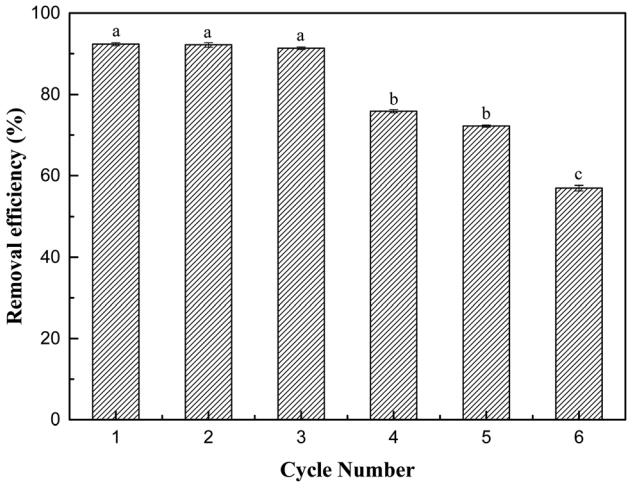

Fig. 11 Reusability of ZIC.

summary, ZIC has a certain anti-interference ability, and the adsorption process is affected by phosphate.

3.3.7 Effect of dissolved organic matter on adsorption. Humic acid is a kind of natural dissolved organic matter with a complex chemical structure. The concentration of humic acid in the natural water environment is usually 0–5 mg L^{-1}.[46] The effect of different concentrations of humic acid on the adsorption of Sb(v) on ZIC is shown in Fig. 10. Due to the unique surface properties and functional groups of humic acid, Sb(v) easily binds to the surface of humic acid, which affects the adsorption effect.[47] With increasing humic acid concentration, the removal rate of Sb(v) gradually decreased. When the concentration of humic acid reached 10 mg L^{-1}, the removal rate of Sb(v) by ZIC decreased from 94.47% to 59.18%. Humic acid may occupy part of the adsorption sites, thereby affecting the adsorption process. Previous studies have found that there are binding interactions between humus and negatively charged metal ions that form complexes.[48] The results showed that ZIC has strong anti-interference ability and is limited by humic acid. It can resist the negative effects of coexisting inorganic and organic substances on adsorption, which illustrates the application potential of ZIC in actual wastewater treatment.

3.3.8 Reusability analysis. Considering the practical application of ZIC, if the adsorbent has good reuse ability, the resource cost can be reduced. ZIC has a higher affinity for hydroxyl groups in alkaline environments than Sb(v), and sodium-hydroxide solution (0.1 M) can be used as a desorption agent to evaluate the reusability of ZIC.[49] Fig. 11 shows that after the adsorbent is recycled three times, the removal rate of Sb(v) by ZIC ranges from 91.33 to 92.33%. After 4–6 recycling cycles, the removal rate decreases with an increase in the number of reuses. In the sixth cycle, the removal rate decreases to 57%. The results show that ZIC has a certain degree of reusability, and it has a good adsorption effect within three repeated uses. This indicates that ZIC has practical prospects for wastewater treatment.

3.4 Adsorption mechanisms

In this study, the adsorption environment of Sb(v) is solution pH = 4.0–10.0. At this time, Sb(v) mainly exists in the aqueous solution in the form of $H_2SbO_4^-$ and $Sb(OH)_6^-$.[2] To increase the electrostatic attraction to Sb(v), it may be necessary to add hydrogen ions to the environment. ZIC is positively charged through protonation in an acidic environment, and Sb(v) is adsorbed on ZIC through electrostatic interactions and ion exchange. If the metal on the adsorbent is denoted as M, the electrostatic interaction between the protonated ZIC surface and Sb(v) can be expressed as:[3,30]

$$M - OH + H^+ \leftrightarrow M - OH_2^+$$

$$M - OH_2^+ + H_2SbO_4^- \leftrightarrow (M - OH_2)^+[H_2SbO_4]^-$$

$$M - OH_2^+ + Sb(OH)_6^- \leftrightarrow (M - OH_2)^+[Sb(OH)_6]^-$$

The ion exchange mechanism can be expressed as:

$$M - OH + H_2SbO_4^- \leftrightarrow M - O - H_2SbO_4 + OH^-$$

$$M - OH + Sb(OH)_6^- \leftrightarrow M - O - Sb(OH)_5 + H_2O$$

$$2(M - OH) + Sb(OH)_6^- \leftrightarrow 2(M - O) - Sb(OH)_4 + 2H_2O$$

Under alkaline conditions, with the increase in hydroxyl groups, the deprotonation of the adsorbent surface, and the strong competition between hydroxide and Sb(v), the electrostatic attraction between the anion and adsorbent is negligible.[50] As a result, the removal rate of Sb(v) decreases as the pH value decreases, and the adsorption process is only controlled by ion exchange.

The FT-IR spectra before and after adsorption of Sb(v) on ZIF are shown in Fig. 12. Since the infrared absorption peaks of metal oxides often appear at low wavenumbers and are not very characteristic,[3] the infrared spectrum absorption peaks before adsorption are dominated by activated carbon: corresponding to the OH-stretching vibration peak at 3444 cm^{-1};

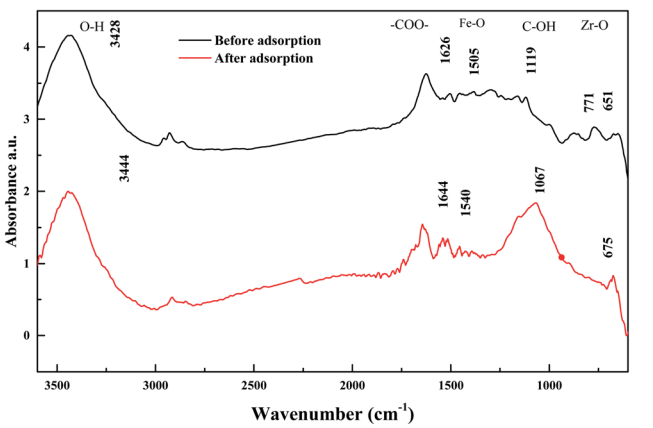

Fig. 12 FT-IR spectra before and after the adsorption of Sb(v) on ZIC.

© 2021 The Author(s). Published by the Royal Society of Chemistry

Open Access Article. Published on 20 September 2021. Downloaded on 2/13/2026 11:42:16 PM.
This article is licensed under a Creative Commons Attribution-NonCommercial 3.0 Unported Licence.

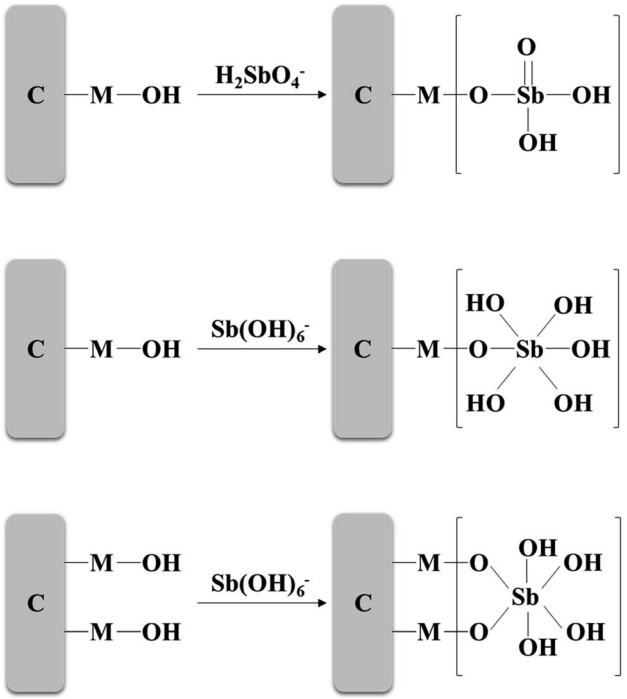

Fig. 13 Adsorption mechanisms of Sb(v) adsorption.

corresponding to the antisymmetric-stretching vibration peak and symmetric-stretching vibration peak of –COO– in carboxylate at 1644 cm^{-1} and 1540 cm^{-1}, respectively; corresponding to the C–OH-stretching vibration peak at 1067 cm^{-1}; and corresponding to metal-oxide M-O vibrations at 675 cm^{-1}. The infrared spectrum of ZIC after adsorption showed that the OH-stretching vibration peak moved to 3428 cm^{-1},[51] the antisymmetric-stretching vibration peak and the symmetric-stretching vibration peak of –COO– moved to 1626 cm^{-1} and 1505 cm^{-1},[52] respectively, the C–OH-stretching vibration peak moved to 1119 cm^{-1},[53] and the M-O vibration peak moved to 651 cm^{-1}.[50] Comparing the infrared spectra before and after the adsorption of Sb(v), it can be found that the peak strength at 1067 cm^{-1} is significantly weakened, and the peak shape changes, indicating that chemical bonds such as –COOH or C–OH in the activated carbon may participate in the Sb adsorption process.[41] A new peak appears at 771 cm^{-1}. According to relevant studies, this peak is the Sb–O curved band formed after ZIC adsorption of Sb(v), which confirms the coordination exchange reaction between Sb(v) and hydroxyl groups.[3] In addition, the absorption peak of metal oxides below 800 cm^{-1} changes significantly, indicating that metal oxides are also involved in the adsorption process of Sb(v), and the adsorption mechanism may be based on water or O–H on the surface of the metal oxides.[54]

In summary, the removal process of Sb(v) by ZIC can be realized by specific adsorption and nonspecific adsorption. On the one hand, as shown in Fig. 13, the hydroxyl groups on the surface of ZIC and Sb(v) undergo coordination exchange to form bidentate binuclear and mononuclear complexes.[55] Finally, the removal of Sb(v) is realized, and this reaction belongs to specific adsorption. On the other hand, ZIC is positively charged due to protonation and can be combined with pollutant ions through electrostatic interactions to achieve the removal of Sb(v), which is nonspecific adsorption.

4. Conclusions

In this study, we successfully prepared an adsorbent with activated carbon as a carrier to support nanometre-zirconium iron oxide and used it to adsorb Sb(v) in aqueous solution. ZIC proved to be an effective composite adsorbent. It not only combines the advantages of good selective adsorption and large adsorption capacity of inorganic adsorbents but also exerts the advantages of organic-carrier, activated-carbon materials, such as large specific surface area and easy separation. In batch experiments, the removal rate of Sb(v) reached 97.82%, and the theoretical maximum adsorption capacity was 11.80 mg g^{-1}. ZIC has a certain resistance to the interference of inorganic ions. The adsorption form is multimolecular-layer adsorption, the adsorption process is an endothermic reaction, and chemical adsorption is dominant in the adsorption mechanism. ZIC has good removal efficiency and is reusable, which indicates that ZIC has prospects for practical wastewater treatment.

Conflicts of interest

There are no conflicts of declare.

Acknowledgements

This research was supported by the National Natural Science Foundation of China (grant number U2006212).

References

1 M. He, *et al.*, Antimony pollution in China, *Sci. Total Environ.*, 2012, **421–422**, 41–50.
2 I. Herath, M. Vithanage and J. Bundschuh, Antimony as a global dilemma: Geochemistry, mobility, fate and transport, *Environ. Pollut.*, 2017, **223**, 545–559.
3 W. Zhang, *et al.*, Removal of antimonite and antimonate from water using Fe-based metal-organic frameworks: The relationship between framework structure and adsorption performance, *J. Environ. Sci.*, 2019, **86**, 213–224.
4 P. Navarro and F. J. Alguacil, Adsorption of antimony and arsenic from a copper electrorefining solution onto activated carbon, *Hydrometallurgy*, 2002, **66**(1), 101–105.
5 X. Long, *et al.*, A review of removal technology for antimony in aqueous solution, *J. Environ. Sci.*, 2020, **90**, 189–204.
6 H. Bessaies, *et al.*, Characterization and physicochemical aspects of novel cellulose-based layered double hydroxide nanocomposite for removal of antimony and fluoride from aqueous solution, *J. Environ. Sci.*, 2021, **102**, 301–315.
7 J. Deng, *et al.*, Different adsorption behaviors and mechanisms of a novel amino-functionalized hydrothermal biochar for hexavalent chromium and pentavalent antimony, *Bioresour. Technol.*, 2020, **310**, 123438.

© 2021 The Author(s). Published by the Royal Society of Chemistry

Open Access Article. Published on 20 September 2021. Downloaded on 2/13/2026 11:42:16 PM. This article is licensed under a Creative Commons Attribution-NonCommercial 3.0 Unported Licence.

8 Y. Sun, *et al.*, The influences of iron characteristics, operating conditions and solution chemistry on contaminants removal by zero-valent iron: A review, *Water Res.*, 2016, **100**, 277–295.
9 Z. Qi, *et al.*, Synthesis of Ce(III)-doped Fe3O4 magnetic particles for efficient removal of antimony from aqueous solution, *J. Hazard. Mater.*, 2017, **329**, 193–204.
10 X. Li, X. Dou and J. Li, Antimony(v) removal from water by iron-zirconium bimetal oxide: Performance and mechanism, *J. Environ. Sci.*, 2012, **24**(7), 1197–1203.
11 A. U. Rajapaksha, *et al.*, Engineered/designer biochar for contaminant removal/immobilization from soil and water: Potential and implication of biochar modification, *Chemosphere*, 2016, **148**, 276–291.
12 N. Sahu, J. Singh and J. R. Koduru, Removal of arsenic from aqueous solution by novel iron and iron–zirconium modified activated carbon derived from chemical carbonization of Tectona grandis sawdust: Isotherm, kinetic, thermodynamic and breakthrough curve modelling, *Environ. Res.*, 2021, **200**, 111431.
13 J. Wang, *et al.*, Insight into the effect of structural characteristics of magnetic ZrO2/Fe3O4 nanocomposites on phosphate removal in water, *Mater. Chem. Phys.*, 2020, **249**, 123024.
14 Y. Wang, *et al.*, Enhanced adsorption of hexavalent chromium from aqueous solutions on facilely synthesized mesoporous iron–zirconium bimetal oxide, *Colloids Surf., A*, 2015, **481**, 133–142.
15 B. Chen, *et al.*, Facile synthesis of mesoporous Ce–Fe bimetal oxide and its enhanced adsorption of arsenate from aqueous solutions, *J. Colloid Interface Sci.*, 2013, **398**, 142–151.
16 Y. Yin, *et al.*, Adsorption of arsenic by activated charcoal coated zirconium-manganese nanocomposite: Performance and mechanism, *Colloids Surf., A*, 2019, **575**, 318–328.
17 H. Cui, *et al.*, Strong adsorption of arsenic species by amorphous zirconium oxide nanoparticles, *J. Ind. Eng. Chem.*, 2012, **18**(4), 1418–1427.
18 L. Yuan, *et al.*, Adsorption and mechanistic study for phosphate removal by magnetic Fe3O4-doped spent FCC catalysts adsorbent, *Chemosphere*, 2019, **219**, 183–190.
19 S. M. Prabhu, P. Koilraj and K. Sasaki, Synthesis of sucrose-derived porous carbon-doped ZrxLa1-xOOH materials and their superior performance for the simultaneous immobilization of arsenite and fluoride from binary systems, *Chem. Eng. J.*, 2017, **325**, 1–13.
20 F. Long, *et al.*, Removal of phosphate from aqueous solution by magnetic Fe–Zr binary oxide, *Chem. Eng. J.*, 2011, **171**(2), 448–455.
21 X. Dou, *et al.*, Identification of Fe and Zr oxide phases in an iron-zirconium binary oxide and arsenate complexes adsorbed onto their surfaces, *J. Hazard. Mater.*, 2018, **353**, 340–347.
22 X. Zhao, *et al.*, Utilization of gel-type polystyrene host for immobilization of nano-sized hydrated zirconium oxides: A new strategy for enhanced phosphate removal, *Chemosphere*, 2021, **263**, 127938.
23 M. A. Rahman, *et al.*, Removal of arsenate from contaminated waters by novel zirconium and zirconium-iron modified biochar, *J. Hazard. Mater.*, 2021, **409**, 124488.
24 S. A. Chaudhry, *et al.*, Fe(III)–Sn(IV) mixed binary oxide-coated sand preparation and its use for the removal of As(III) and As(V) from water: Application of isotherm, kinetic and thermodynamics, *J. Mol. Liq.*, 2016, **224**, 431–441.
25 L. Song, *et al.*, Facile one-step fabrication of carboxymethyl cellulose based hydrogel for highly efficient removal of Cr(VI) under mild acidic condition, *Chem. Eng. J.*, 2019, **369**, 641–651.
26 M. Yaseen, *et al.*, Fabrication of rGO-CuO and/or Ag2O nanoparticles incorporated polyvinyl acetate based mixed matrix membranes for the removal of Cr6+ from anti-corrosive paint industrial wastewater, *J. Environ. Chem. Eng.*, 2021, **9**(2), 105151.
27 H. Yaqi, *et al.*, In Situ Co-Precipitation Formed Highly Water-Dispersible Magnetic Chitosan Nanopowder for Removal of Heavy Metals and Its Adsorption Mechanism, *ACS Sustainable Chem. Eng.*, 2018, **6**(12), 16754–16765.
28 G. Zhu, *et al.*, A biochar supported magnetic metal organic framework for the removal of trivalent antimony, *Chemosphere*, 2021, 131068.
29 W. Guo, *et al.*, Synthesis of Fe3O4 magnetic nanoparticles coated with cationic surfactants and their applications in Sb(V) removal from water, *Sci. Total Environ.*, 2020, **710**, 136302.
30 K. Zhou, *et al.*, Development of polymeric iron/zirconium-pillared clinoptilolite for simultaneous removal of multiple inorganic contaminants from wastewater, *Chem. Eng. J.*, 2018, **347**, 819–827.
31 N. K. Niazi, *et al.*, Arsenic removal by perilla leaf biochar in aqueous solutions and groundwater: An integrated spectroscopic and microscopic examination, *Environ. Pollut.*, 2018, **232**, 31–41.
32 Q. Liang, *et al.*, Fast and selective removal of Cr(VI) from aqueous solutions by a novel magnetic Cr(VI) ion-imprinted polymer, *J. Mol. Liq.*, 2017, **248**, 767–774.
33 J. Li, *et al.*, Antimony contamination, consequences and removal techniques: A review, *Ecotoxicol. Environ. Saf.*, 2018, **156**, 125–134.
34 X. Zhao, *et al.*, Antimonate and antimonite adsorption by a polyvinyl alcohol-stabilized granular adsorbent containing nanoscale zero-valent iron, *Chem. Eng. J.*, 2014, **247**, 250–257.
35 J. Luo, *et al.*, Removal of Antimonite (Sb(III)) and Antimonate (Sb(V)) from Aqueous Solution Using Carbon Nanofibers That Are Decorated with Zirconium Oxide (ZrO2), *Environ. Sci. Technol.*, 2015, **49**(18), 11115–11124.
36 J. Xi, M. He and L. Kong, Adsorption of antimony on kaolinite as a function of time, pH, HA and competitive anions, *Environ. Earth Sci.*, 2016, **75**(2), 136.
37 J. Xi, M. He and C. Lin, Adsorption of antimony(III) and antimony(V) on bentonite: Kinetics, thermodynamics and anion competition, *Microchem. J.*, 2011, **97**(1), 85–91.

© 2021 The Author(s). Published by the Royal Society of Chemistry

Open Access Article. Published on 20 September 2021. Downloaded on 2/13/2026 11:42:16 PM.
This article is licensed under a Creative Commons Attribution-NonCommercial 3.0 Unported Licence.

38 Z. Qi, *et al.*, Enhanced Oxidative and Adsorptive Capability towards Antimony by Copper-doping into Magnetite Magnetic particles, *RSC Adv.*, 2016, **6**, 66990–67001.

39 J.-P. Zou, *et al.*, Three-Dimensional Reduced Graphene Oxide Coupled with Mn3O4 for Highly Efficient Removal of Sb(III) and Sb(V) from Water, *ACS Appl. Mater. Interfaces*, 2016, **8**(28), 18140–18149.

40 J. Luo, *et al.*, Antimony Removal from Aqueous Solution Using Novel α-MnO2 Nanofibers: Equilibrium, Kinetic, and Density Functional Theory Studies, *ACS Sustainable Chem. Eng.*, 2017, **5**(3), 2255–2264.

41 S. I. Siddiqui and S. A. Chaudhry, Nanohybrid composite Fe2O3-ZrO2/BC for inhibiting the growth of bacteria and adsorptive removal of arsenic and dyes from water, *J. Cleaner Prod.*, 2019, **223**, 849–868.

42 C.-H. Liu, *et al.*, Mechanism of Arsenic Adsorption on Magnetite Nanoparticles from Water: Thermodynamic and Spectroscopic Studies, *Environ. Sci. Technol.*, 2015, **49**(13), 7726–7734.

43 H. Lu, *et al.*, Simultaneous removal of arsenate and antimonate in simulated and practical water samples by adsorption onto Zn/Fe layered double hydroxide, *Chem. Eng. J.*, 2015, **276**, 365–375.

44 L. Wang, *et al.*, Mechanism of enhanced Sb(V) removal from aqueous solution using chemically modified aerobic granules, *J. Hazard. Mater.*, 2015, **284**, 43–49.

45 S. C. Wilson, *et al.*, The chemistry and behaviour of antimony in the soil environment with comparisons to arsenic: A critical review, *Environ. Pollut.*, 2010, **158**(5), 1169–1181.

46 X. Liu, *et al.*, Inhibition of urease activity by humic acid extracted from sludge fermentation liquid, *Bioresour. Technol.*, 2019, **290**, 121767.

47 S. Tserenpil and C.-Q. Liu, Study of antimony (III) binding to soil humic acid from an antimony smelting site, *Microchem. J.*, 2011, **98**(1), 15–20.

48 Y. Zhang, Y. Wang and I. Angelidaki, Alternate switching between microbial fuel cell and microbial electrolysis cell operation as a new method to control H2O2 level in Bioelectro-Fenton system, *J. Power Sources*, 2015, **291**, 108–116.

49 L. Wang, *et al.*, Enhanced antimonate (Sb(V)) removal from aqueous solution by La-doped magnetic biochars, *Chem. Eng. J.*, 2018, **354**, 623–632.

50 W. Xiong, *et al.*, Adsorption of phosphate from aqueous solution using iron-zirconium modified activated carbon nanofiber: Performance and mechanism, *J. Colloid Interface Sci.*, 2017, **493**, 17–23.

51 L. S. Thakur, H. Goyal and P. Mondal, Simultaneous removal of arsenic and fluoride from synthetic solution through continuous electrocoagulation: Operating cost and sludge utilization, *J. Environ. Chem. Eng.*, 2019, **7**(1), 102829.

52 P. Duan, *et al.*, Amine-crosslinked Shaddock Peel embedded with hydrous zirconium oxide nano-particles for selective phosphate removal in competitive condition, *J. Taiwan Inst. Chem. Eng.*, 2017, **80**, 650–662.

53 L. Verma, *et al.*, As(III) and As(V) removal by using iron impregnated biosorbents derived from waste biomass of Citrus limmeta (peel and pulp) from the aqueous solution and ground water, *J. Environ. Manage.*, 2019, **250**, 109452.

54 X. Feng, *et al.*, Nano ferric oxide adsorbents with self-acidification effect for efficient adsorption of Sb(V), *Chemosphere*, 2021, **272**, 129933.

55 M. Vithanage, *et al.*, Surface complexation modeling and spectroscopic evidence of antimony adsorption on iron-oxide-rich red earth soils, *J. Colloid Interface Sci.*, 2013, **406**, 217–224.

© 2021 The Author(s). Published by the Royal Society of Chemistry